

Voracious vortexes in cataclysmic variables

Multi-epoch tomographic study of HT Cassiopeia

V. V. Neustroev¹, S. V. Zharikov², and N. V. Borisov³

¹ Astronomy and Space Physics, PO Box 3000, FIN-90014 University of Oulu, Finland
e-mail: vitaly@neustroev.net

² Instituto de Astronomía, Universidad Nacional Autónoma de México, Apdo. Postal 877, Ensenada, 22800 Baja California, México

³ Special Astrophysical Observatory of the Russian AS, Nizhnij Arkhyz, Karachaevo-Cherkesia 369167, Russia

Received April 20, 2015; accepted ?

ABSTRACT

We present multi-epoch, time-resolved optical spectroscopic observations of the dwarf nova HT Cas, obtained during 1986, 1992, 1995 and 2005 with the aim to study the properties of emission structures in the system. We determined that the accretion disc radius, measured from the double-peaked emission line profiles, is persistently large and lies within the range of $0.45\text{--}0.52a$, where a is the binary separation. This is close to the tidal truncation radius $r_{\text{max}}=0.52a$. This result contradicts with previous radius measurements. An extensive set of Doppler maps has revealed a very complex emission structure of the accretion disc. Apart from a ring of disc emission, the tomograms display at least three areas of enhanced emission: the hot spot from the area of interaction between the gas stream and the disc, which is superposed on the elongated spiral structure, and the extended bright region on the leading side of the disc, opposite to the location of the hot spot. The position of the hot spot in all the emission lines is consistent with the trajectory of the gas stream. However, the peaks of emission are located in the range of distances $0.22\text{--}0.30a$, which are much closer to the white dwarf than the disc edge. This suggests that the outer disc regions have a very low density, allowing the gas stream to flow almost freely before it starts to be seen as an emission source. We have found that the extended emission region in the leading side of the disc is always observed at the very edge of the large disc. Observations of other cataclysmic variables, which show a similar emission structure in their tomograms, confirm this conclusion. We propose that the leading side bright region is caused by irradiation of tidally thickened sectors of the outer disc by the white dwarf and/or hot inner disc regions.

Key words. methods: observational – accretion, accretion discs – binaries: close – novae, cataclysmic variables – stars:individual: HT Cas

1. Introduction

Cataclysmic variables (CVs) are close interacting binary systems consisting of a white dwarf (WD) as primary and a low-mass main-sequence star or a brown dwarf as secondary component (Warner 1995, and references therein). The Roche-lobe filling secondary loses matter via the inner Lagrangian point to the primary. In the absence of a strong magnetic field, the material transferred from the donor star forms an accretion disc around the WD and gradually spirals down onto its surface and eventually accretes.

Typical optical spectra of CVs are dominated by emission lines of hydrogen and neutral helium series, formed in the accretion disc. Lines of other species, such as those from singly ionized helium, calcium and iron are also often seen (Williams 1983; Honeycutt et al. 1987). The emission lines of CVs with a moderately high orbital inclination are usually very broad with a full-width velocity over several thousand km s^{-1} and have a double-peaked profile resulting from the Doppler shift of matter rotating in a Keplerian disc (Smak 1969, 1981; Horne & Marsh 1986).

Although the accretion disc is the dominant light source in CVs, many examples show that other emission components may distort the originally symmetric line profile. It is commonly observed that the intensities of the red and blue peaks of the double-

peaked profiles are variable with the orbital period phase (Greenstein & Kraft 1959). The trailed spectra often show a narrow emission component which moves from one line hump to the other and back during the course of the orbital period, having the form of an “S-wave” (Kraft et al. 1962). This S-wave component is usually attributed to a region of high temperature and luminosity at the outer edge of the accretion disc that is caused by its interaction with the inflowing gas stream (Smak 1970). This interpretation is supported by the phasing of the S-wave component, which crosses from blue-shifted to red-shifted around phase $0.8\text{--}0.9$, which corresponds closely to the expected phasing of this bright area. For the remainder of this paper, we use the outdated term “the hot spot” to refer to the area of interaction between the gas stream and the accretion disc, in order to distinguish the latter with other bright spots on accretion discs.

It soon appeared that other sources of emission may also be present in an accretion disc. In 1981 Young et al. reported the spectroscopic study of the dwarf nova HT Cas, which spectra showed unusual behaviour: “*The blue wing is stronger near phase 0.0 and the red one stronger at phase 0.5. This resembles the variations to be expected from an S-wave, but is 180° out of phase!*”. The identification of this and other detected emission spots, the phasing of which does not agree with that expected for the hot spot model, was ambiguous.

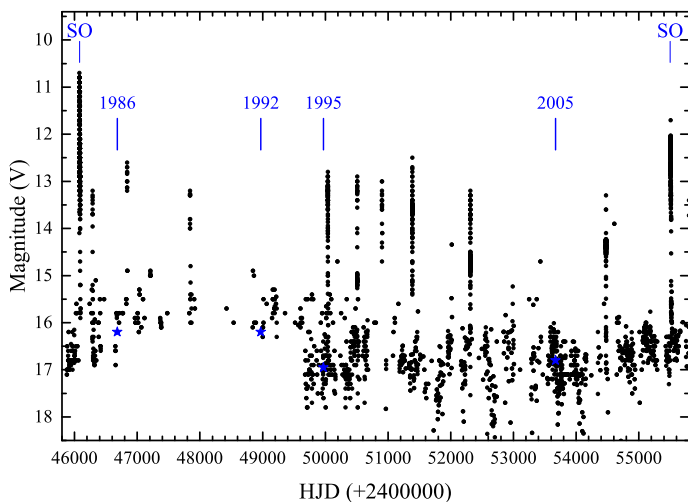


Fig. 1. AAVSO light curve of HT Cas between two superoutbursts in 1985 and 2010, marked by “SO”. The blue stars represent averaged magnitudes of the star during our spectroscopic observations.

The development of Doppler tomography opened up a new regime for studying accretion structures in interacting binaries (Marsh & Horne 1988). This technique uses the information encoded in spectral line profiles taken at different orbital phases to calculate a distribution of emission over the binary. Doppler tomography is now widely used to study interacting binary systems, the tomograms of many dozens CVs were produced to date. Although a Doppler map is subject to interpretation since it is created in velocity space, the predicted location of different binary system components in spatial coordinates can easily be translated into velocity coordinates and hence, compared with the map. Besides the hot spot, this approach helps to identify an irradiated part of secondary stars (Marsh & Horne 1990), spiral structures in accretion discs (Steehls et al. 1997), accretion flows in polars (Heerlein et al. 1999), and a “reversed bright spot” caused by the deflected gas stream flow that passes above the disc and hits its back (Neustroev 1998; Neustroev et al. 2011).

Nevertheless, there are observed emission structures which still have no plausible explanation. One of the most mysterious is a bright spot on the leading side of the disc, *opposite* to the usual location of the hot spot. In trailed spectra it produces an S-wave which crosses from blue-shifted to red-shifted around phase 0.5. In Doppler images it is situated in the bottom-right part of the map. This place is far from the region of interaction between the stream and the disc particles. The presence of the leading side bright spot was reported for RR Pic (Schmidtobreick et al. 2003), WX Cet (Tappert et al. 2003), BZ UMa (Neustroev et al. 2006), VW Hyi (Smith et al. 2006), 1RXS J180834.7+101041 (Yakin et al. 2011), V406 Vir (Aviles et al. 2010), EZ Lyn (Zharikov et al. 2013), V2051 Oph (Papadaki et al. 2008; Longa-Peña et al. 2015). This list is by far not complete. A rough statistical analysis applied to a sample of 68 CVs with published emission line profile studies showed that the presence of the leading side bright spot is not an exception but a frequent phenomenon (Tappert & Hanuschik 2001), the source of which has not yet been found.

This motivated us to perform a detailed study of the properties of emission structures in HT Cas, seemingly the first CV that has been noticed to have a bright spot in the leading side of the accretion disc (Young et al. 1981). In this paper we present and discuss the medium-resolution spectroscopic data obtained during 1986, 1992, 1995 and 2005.

2. HT Cassiopeiae

HT Cas was discovered by Hoffmeister (1943) and classified as a U Gem type star with brightness varying between 13.0 and 16.5 mag. The eclipses of HT Cas were discovered by Bond (1978) and extensively observed by Patterson (1981), who derived an orbital period of 1.77 h for the system. Borges et al. (2008) reported that the orbital period shows period changes of semi-amplitude ~ 40 s which seems to repeat on a time-scale of about 36 yr. The system is characterized by very rare outbursts with mean intervals of 400 days (Wenzel 1987), suggesting an extremely low mass-transfer rate in the system. Moreover, the outbursts occur rather irregularly, e.g. no outbursts were observed from 1989 to 1995 (Kato et al. 2012). In January 1985, Zhang et al. (1986) observed HT Cas in a long and bright outburst and detected superhumps in the light curve of the object, confirming its classification as an SU UMa star. Only two superoutburst are documented for HT Cas. The next one after 1985 was observed only in 2010 (Kato et al. 2012). The system is also known to exhibit large-amplitude, long-time-scale quiescent light variations, from about 15.9 to 17.7 mag (Robertson & Honeycutt 1996, see also Fig. 1).

Eclipses provide a great opportunity to measure system parameters and to study the accretion disc structure in detail. Patterson (1981) even called HT Cas “the Rosetta Stone of dwarf novae”, yet this system might appear to be too atypical for dwarf novae. The light curves and eclipse profiles of HT Cas strongly vary (Patterson 1981; Zhang et al. 1986; Wood et al. 1995). They predominantly show the deep eclipse of the WD, also visible in X-rays (Wood et al. 1995), but the accretion disc component is usually weak and sometimes absent. Orbital humps – hot spot modulations – are rarely seen in quiescence. However, the brightness of the hot spot increased significantly during the 2010 superoutburst (Bąkowska & Olech 2014).

The system parameters for HT Cas are usually taken from Horne et al. (1991): $M_1 = 0.61 \pm 0.04 M_\odot$, $M_2 = 0.09 \pm 0.02 M_\odot$, $q = 0.15 \pm 0.03$, $i = 81.0 \pm 1.0^\circ$. They are based on the derived parameters of a WD eclipse. Several authors studied the accretion disc in HT Cas with the multicolour eclipse mapping technique. These studies showed that the quiescent disc has a flat brightness temperature profile (5000–7000 K) (Wood et al. 1992) and is probably patchy (Vrielmann et al. 2002). Using a similar approach, Feline et al. (2005) revealed changes in the quiescent accretion disc structure, possibly related to variations in the mass transfer rate from the secondary star. There has been controversy in the literature over the optical thickness of the accretion disc in HT Cas. Zhang et al. (1986) found that the disc is optically thick, Vrielmann et al. (2002) argued that the disc is moderately optically thin, but becomes optically thick near the WD, while Wood et al. (1992) and Feline et al. (2005) claimed that the disc is optically thin in both its inner and outer regions.

The optical spectrum of HT Cas is typical for a high-inclination dwarf nova, with strong double-peaked emission lines of hydrogen and neutral helium. First spectroscopic observations were made by Rafanelli (1979), who presented a few photographic spectra. Unfortunately, despite a rich history of photometric investigations, HT Cas has been almost neglected with optical high- or medium-resolution spectroscopy. The most recent time-resolved spectroscopic study in the blue wavelength range was presented almost 35 years ago by Young et al. (1981). In particular, they found that the variability of the Balmer emission lines cannot be explained by the canonical hot spot model and that the semi-amplitude K_1 of their radial-velocity variations is about 115 km s^{-1} . Yet the radial velocity curves are

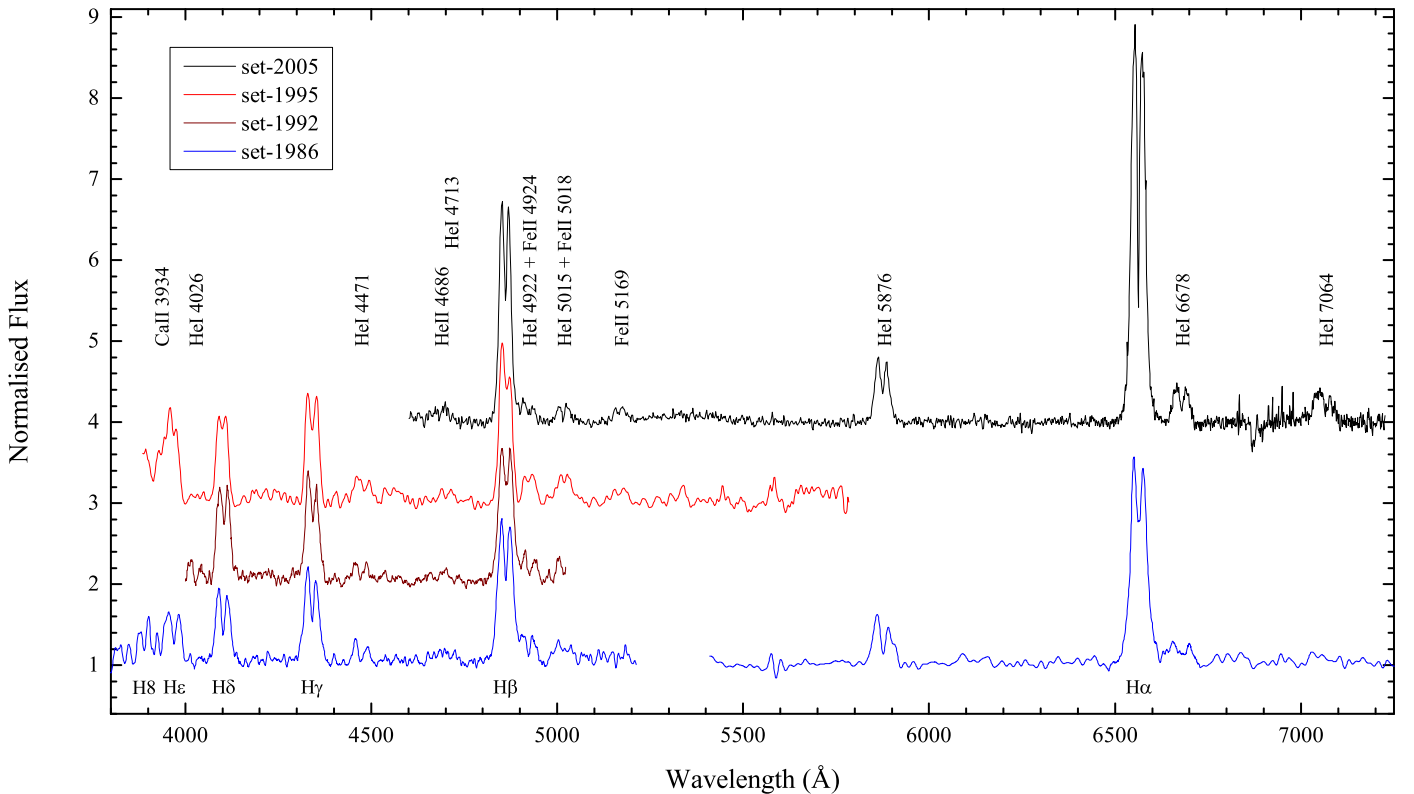


Fig. 2. Combined and continuum-normalised out-of-eclipse spectra of HT Cas for each epoch of observation. Spectra shifted vertically to prevent overlap.

Table 1. Log of spectroscopic observations of HT Cas

Set	Date	Telescope/ Instrument	λ range (Å)	Exp.Time (sec)	Number of exps.	Duration (hours)
Set-1986	1986-Sep-08	6.0 m / SP-124	3600–5500	300	15	1.77
	1986-Sep-09	6.0 m / SP-124	5400–7300	360	16	2.12
Set-1992	1992-Dec-16	6.0 m / SP-124	3600–5500	300	14	1.41
Set-1995	1995-Sep-09	6.0 m / SP-124	3860–5800	180	58	3.54
Set-2005	2005-Oct-29	2.1 m / B&Ch	4600–6700	293	40	3.54
	2005-Oct-31	2.1 m / B&Ch	6150–7225	293	40	3.54

shifted by 30° relative to the eclipse. Horne et al. (1991) concluded in their work that the K_1 velocity of 115 km s^{-1} is unreliable and predicted K_1 to be $58 \pm 11 \text{ km s}^{-1}$. This was neither confirmed nor denied until now. There was one more spectroscopic study of HT Cas performed by Marsh (1990) with the low-resolution data. Marsh was able to detect absorption lines from the $M5.4 \pm 0.3$ secondary star and to measure its radial velocity semi-amplitude $K_2 = 430 \pm 25 \text{ km s}^{-1}$. Nevertheless, no attempt was made to study the emission lines in detail and to derive K_1 .

Among other peculiar characteristics of HT Cas, there is an unusually small radius of the accretion disc R_d as inferred by many researchers (Zhang et al. 1986; Horne et al. 1991; Vrielmann et al. 2002; Feline et al. 2005). A typical value of R_d in quiescence was measured to be $\approx 0.23a$. This is only a bit larger than the circularization radius ($0.195a$, Verbunt & Rappaport 1988) which determines the theoretically allowed minimal accretion disc radius. We note that most of those measurements of R_d were based on the position of the hot spot. We seriously doubt this approach and show in Section 5.1 that the position of the hot

spot does not always give reliable estimates for the accretion disc radius.

3. Observations and Data reduction

The spectra presented here were obtained during four observing runs in 1986, 1992, 1995 and 2005. In order to check the photometric state of HT Cas, during each set of spectroscopic observations we also obtained a few photometric measurements on accompanying telescopes. These observations indicate that though HT Cas has always remained in quiescence, its brightness was changing substantially. During the observations in 1986 and 1992 the V magnitude was about 16.2 mag, whereas in 1995 and 2005 it was ~ 17.0 and ~ 16.8 mag, respectively (Fig. 1).

The first three observations were conducted in 1986, 1992 and 1995 at the Special Astrophysical Observatory of the Russian Academy of Sciences, using a 1024-channel television scanner mounted on the SP-124 spectrograph at the Nasmyth-1 focus of the 6-m telescope (Drabek et al. 1986). The observations in 1986 were taken during two consecutive nights of September 8 and 9, about 20 months after the superoutburst. The spectra were

Table 2. Parameters of the most prominent emission lines in the averaged spectra of HT Cas

Set	Spectral line	Flux (erg s ⁻¹ cm ⁻²)	Relative intensity	FWHM (km s ⁻¹)	Peak-to-peak (km s ⁻¹)	Model parameters		
						V_{out} (km s ⁻¹)	b	$r_{\text{in}}/r_{\text{out}}$
1986	H α		3.50	2130	1120	590 \pm 5	1.59 \pm 0.03	0.06 \pm 0.01
	H β		2.75	2865	1370	620 \pm 21	2.03 \pm 0.08	0.07 \pm 0.01
	H γ		2.10	3030	1450			
	H δ		1.89	3200	1750			
	He I λ 4471		1.28	3150	2090			
	He I λ 4922		1.36		1850			
	He I λ 5015		1.28	3500	2030			
	Fe II λ 5169		1.20					
	He I λ 5876		1.50	2860	1500	690 \pm 9	2.36 \pm 0.03	0.08 \pm 0.01
	He I λ 6678		1.40	2150	1080			
1992	H β		2.68	2720	1360	742 \pm 8	1.42 \pm 0.08	0.06 \pm 0.01
	H γ		2.30	2800	1570			
	H δ		2.20	2990	1520			
	He I λ 4471		1.27		2010			
	He I λ 4922		1.34		1700			
1995	H β		2.75	2440	1250			
	H γ		2.32	2830	1670			
	H δ		2.08	2670	1264			
	He I λ 4471		1.29					
	He I λ 4922		1.34					
	He I λ 5015		1.36					
	Fe II λ 5169		1.18					
2005-n1	H α	8.7 \times 10 ⁻¹⁴	5.55	1960	1070	572 \pm 6	0.81 \pm 0.04	0.04 \pm 0.01
	H β	7.4 \times 10 ⁻¹⁴	3.70	2160	1090	571 \pm 11	1.58 \pm 0.08	0.09 \pm 0.01
	He I λ 4922	6.6 \times 10 ⁻¹⁵	1.21		1520			
	He I λ 5015	6.9 \times 10 ⁻¹⁵	1.20	2340	1260			
	Fe II λ 5169	5.0 \times 10 ⁻¹⁵	1.19		1120			
	He I λ 5876	2.1 \times 10 ⁻¹⁴	1.77	2130	1160	606 \pm 7	1.41 \pm 0.04	0.02 \pm 0.01
	He II λ 4686	4.7 \times 10 ⁻¹⁵	1.15		1640			
2005-n2	H α	1.03 \times 10 ⁻¹³	5.65	1960	920	581 \pm 8	0.95 \pm 0.09	0.06 \pm 0.02
	He I λ 6678	1.0 \times 10 ⁻¹⁴	1.42	2150	1080			
	He I λ 7064	8.8 \times 10 ⁻¹⁵	1.35		1140			

taken in the wavelength ranges of 3600–5210 Å (“blue” spectra) and 5410–7260 Å (“red” spectra) respectively with a dispersion of 1.9 Å channel⁻¹. Corresponding spectral resolution was about 4.5 Å. A total of 15 blue and 16 red spectra were obtained with 300 and 360 sec individual exposures. About 1.0 and 1.25 orbital cycles were covered each night. The observations on 16 December 1992 and 9 September 1995 were conducted with the same dispersion in the blue wavelength range only (4000–5020 Å and 3900–5780 Å, respectively). 14 and 58 spectra with 300 and 180 sec individual exposures were taken during these runs, covering about 0.8 and 2.0 orbital cycles. We note that the 1995 observations were done about 2 months before the normal outburst, which was particularly well observed by Ioannou et al. (1999). Because of electronic focus issues with the TV scanner during the 1995 observations, the spectral resolution of these data degrades rather quickly toward longer wavelengths, especially beyond ~4500 Å. However, the quality of the spectra in shorter wavelengths is still reasonably good and suitable for an analysis. Comparison spectra of HeNeAr lamp were used for the wavelength calibration. No attempt at flux calibration was made for these data. The data reduction of the SAO observations was done using the procedure described by Kniazev (1994). Hereafter we will refer to these data sets as *set-1986*, *set-1992* and *set-1995*.

Further observations were obtained in 2005 during 2 nights of October 29 and 31 at the Observatorio Astronómico Nacional

(OAN SPM) in Mexico on the 2.1-m telescope with the Boller & Chivens spectrograph, equipped with a 24 μ m (1024 \times 1024) SITE CCD chip. The observations on the first night were taken in the wavelength range of 4600–6700 Å with a dispersion of 2.05 Å pixel⁻¹, while the rest of the spectra were obtained in the wavelength range of 6150–7225 Å with a dispersion of 1.05 Å pixel⁻¹. Corresponding spectral resolution was about 4.1 and 2.2 Å, respectively. A total of 40 spectra with 293 sec individual exposures were taken each night, covering exactly 2 orbital periods. Comparison spectra of CuHeNeAr lamp taken during the night were used for the wavelength calibration. Both nights of observations were photometric with the seeing ranged from 1 to 2 arcsec. In order to apply an accurate flux correction, two standard spectrophotometric stars at different airmasses were observed every night. They were selected from Feige110, HR3454 and G191-B2B (Oke 1990). The data reduction was performed using the IRAF environment. We will refer to these data as *set-2005*, sometimes dividing it into *set-2005-n1* and *set-2005-n2* for the first and second nights of observations, if necessary. Log of observations is presented in Table 1.

The orbital phases of the spectra were calculated using the linear ephemeris of Feline et al. (2005). The uncertainties of this ephemeris in the orbital phase at the time of our observations are negligible. For the 2005 data, for which the propagated error is larger, it is less than 2×10^{-4} .

Table 3. Equivalent Widths of HT Cas

Set	Ref.	H α	H β	H γ	H δ	$\lambda 4471$	$\lambda 4922$	$\lambda 5015$	$\lambda 5169$	$\lambda 5876$	$\lambda 6678$	$\lambda 7064$	Magnitude (V)
1980	1	–	77.4	51.0	41.1	11.7	9.2	9.5	–	–	–	–	16.0
1981	2	233.0	98.0	72.8	61.7	16.0	11.0	12.0	12.0	32.0	32.0	–	16.2
1986	3	125.9	82.0	47.9	37.9	10.2	15.0	14.3	7.2	27.4	17.4	–	16.2
1988	4	186.4	–	–	–	–	–	–	–	34.1	17.4	16.1	16.2
1992	3	–	76.1	54.3	48.4	12.0	12.6	–	–	–	–	–	16.2
1995	3	–	69.9	50.7	39.3	14.5	13.3	16.5	8.0	–	–	–	17.0
2005	3	198.5	98.0	–	–	–	7.5	7.9	6.2	30.4	19.7	18.2	16.8

References. (1) Young et al. (1981): the spectra were taken on 1980 August 1; (2) Williams (1983): the spectra were taken on 1981 December 24–27; (3) This paper; (4) Marsh (1990): the spectra were taken on 1988 July 22–24.

Table 4. The Balmer and He I decrements

Set	Ref.	H α /H β	H γ /H β	H δ /H β	He I $\lambda 6678/\lambda 4922$	He I $\lambda 5876/\lambda 4471$	He I $\lambda 5876/\lambda 6678$	H β /He I $\lambda 4922$
1980	1	–	0.66	0.53	–	–	–	8.37
1981	2	2.38	0.74	0.63	2.91	2.00	1.00	8.91
1986	3	1.54	0.58	0.46	1.16	2.69	1.57	5.47
1988	4	–	–	–	–	–	1.96	–
1992	3	–	0.71	0.64	–	–	–	6.03
1995	3	–	0.72	0.56	–	–	–	5.26
2005	3	2.03	–	–	2.63	–	1.54	13.07

References. (1) Young et al. (1981); (2) Williams (1983); (3) This paper; (4) Marsh (1990).

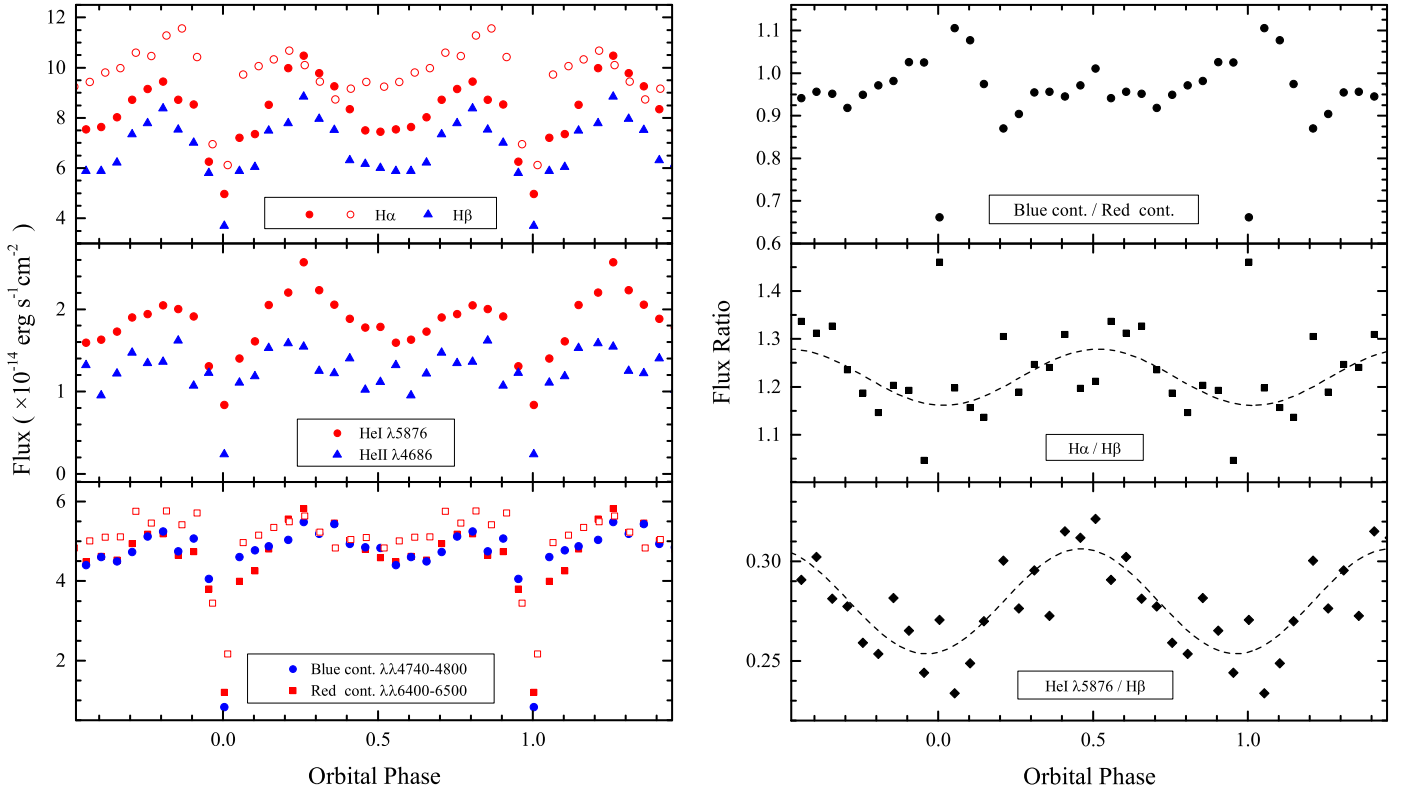


Fig. 3. Left: continuum and emission-line light curves. The filled symbols represent the data from the set-2005-n1, the open symbols are for the set-2005-n2. Right: continuum and emission-line flux ratios.

4. Data analysis and results

4.1. Averaged spectra and their long-term variability

The averaged and continuum-normalised out-of-eclipse spectra of HT Cas, uncorrected for orbital motion, are shown in Fig. 2. Here and elsewhere in this paper, out-of-eclipse phases

are defined as $0.1 \leq \phi \leq 0.9$. The averaged spectra are similar in appearance to that presented by Young et al. (1981) and Williams (1983). They are dominated by extremely strong and broad double-peaked emission lines of the Balmer series. Apart from hydrogen, numerous weaker emission lines of neutral helium and singly ionized iron (Fe II) are present. Also, the high-

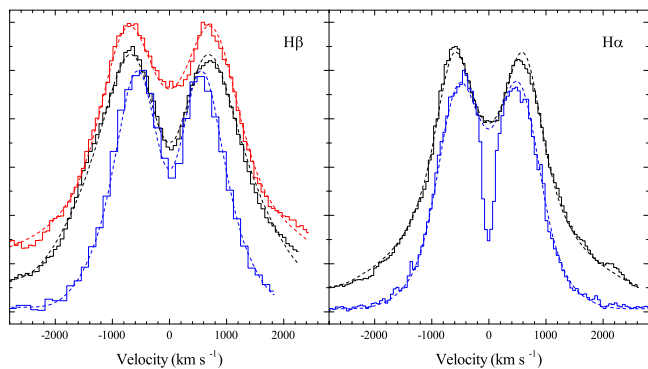


Fig. 4. Averaged profiles of the $H\alpha$ and $H\beta$ emission lines observed in 1992, 1986 and 2005 (red, black and blue lines, respectively) together with the corresponding model fits (dashed lines). The 1992, 1986 and 2005 profiles are shifted vertically by 10 per cent to prevent overlap.

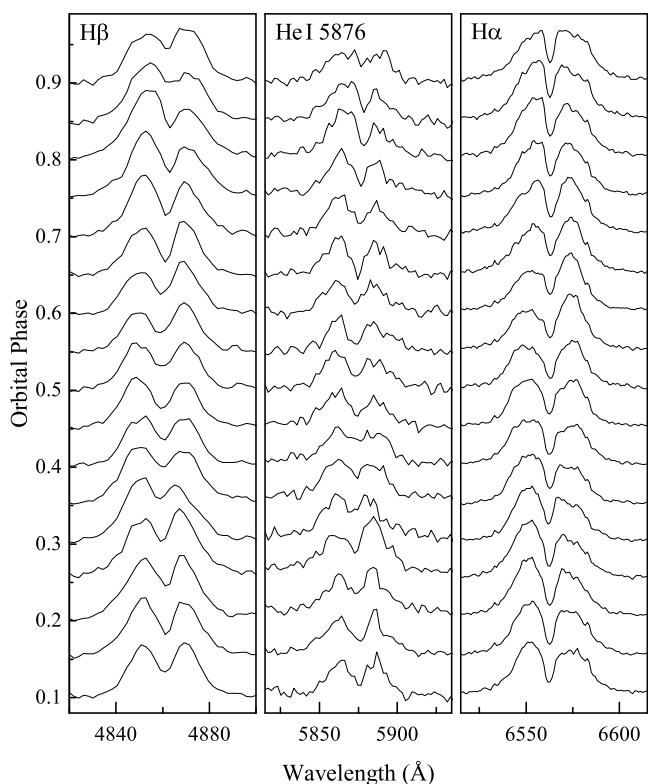


Fig. 5. Evolution of the out-of-eclipse emission line profiles during the set-2005-n1 ($H\beta$ and $He\ I\ 5876$) and the set-2005-n2 ($H\alpha$). The spectra have been ordered according to phase.

excitation line of $He\ II\ \lambda 4686$ is clearly detected. Table 2 outlines different parameters of the most prominent lines measured from the averaged spectra. In Tables 3 and 4 we also separately present the equivalent width (EW) measurements including those available in the literature, and the corresponding Balmer and neutral-helium decrement values, respectively.

A comparison of the averaged spectra from different data sets shows significant quantitative differences between them. There are notable variations in both emission-line strengths and their ratios for different lines. For example, the EW of $H\alpha$ in the set-

1986 is $\sim 126\ \text{\AA}$, but in the set-2005 it reaches almost $200\ \text{\AA}$. The Balmer decrement, being relatively flat in the sets 1992 and 1995, appears rather steep in the set-1986 and especially in the set-2005, indicating optically thin conditions. The decrement within various series of neutral helium lines (e.g., the singlets $\lambda 6678/\lambda 4922$ and triplets $\lambda 5876/\lambda 4471$), the relative strengths of the $He\ I$ triplet and singlet lines (e.g., $\lambda 5876/\lambda 6678$) and the ratio of hydrogen to $He\ I$ strengths have also changed substantially (Table 4). This implies that the opacity and the optical thickness of the disc have varied over time, but these variations do not seem to correlate directly with the system flux (see the last column in Table 3).

4.2. Light and colour curves

The spectra from the set-2005 were used to construct light curves. The blue and red continuum light curves were computed by summing the flux in the wavelength ranges $\lambda\lambda 4740\text{--}4800$ and $\lambda\lambda 6400\text{--}6500\ \text{\AA}$, respectively. The emission-line light curves for $H\alpha$, $H\beta$, $He\ I\ \lambda 5876$ and $He\ II\ \lambda 4686$ were computed by summing the continuum-subtracted flux inside of $\pm 2700\ \text{km s}^{-1}$ window centered at the emission-line wavelengths. The resulting light curves are plotted in Fig. 3 (left-hand panel). Although a non-sufficient phase resolution of the data does not allow us to investigate the eclipse profiles in detail, we are still able to see their most distinctive features. The continuum shows a deep almost symmetrical eclipse, the blue light curve having a deeper eclipse than the red. There is a weak sign of an orbital hump around phase 0.8–0.9, better seen in the blue light, consistent with the presence of the hot spot. The orbital hump is stronger in the Balmer and $He\ I$ lines. The eclipses of the emission lines have a different shape from the continuum, exhibiting a distinctive shoulder during egress. The latter feature is seen in both the Balmer, $He\ I$ and $He\ II$ lines, except for the $H\alpha$ line from the set-2005-n2. We note that even though the continuum flux was nearly the same during two nights of the 2005 observations, the $H\alpha$ line appeared to be slightly stronger on the second night.

Figure 3 (right-hand panel) also shows the flux ratios of the continuum segments and Balmer and $He\ I$ emission lines. The ratio of the blue and red continuum fluxes (an equivalent of a colour index) shows little variations outside of eclipses, but there is a sign of an orbital hump with maximum at phase ~ 0.95 , during which the continuum appears bluer. That is consistent with the presence of the hot spot. The binary becomes much redder in the middle of the eclipse. The $H\alpha/H\beta$ and $He\ I\ \lambda 5876/H\beta$ ratios show synchronous sinusoidal variations, with the lowest value being also observed at phase 0.95–1.0. The $H\alpha/H\beta$ ratio varies by ~ 10 per cent around a mean value and there is a notable zig-zag jump in the first half of the eclipse. The $He\ I\ \lambda 5876/H\beta$ ratio varies considerably by a factor of ~ 2 more than the $H\alpha/H\beta$. However, the data show no clear evidence for a jump during the eclipse.

4.3. Accretion disc parameters from modelling of the emission line profiles

All emission lines exhibit, in the averaged spectra, slightly asymmetric double-peaked profiles, with a stronger blue peak than the red one. The lines are very broad with a FWZI of up to $5\text{--}6$ thousand km s^{-1} and a peak-to-peak separation of $\gtrsim 1100\ \text{km s}^{-1}$ (in $H\alpha$) which increases monotonically towards the higher order Balmer lines. These properties suggest the origin of emission lines in an accretion disc (Smak 1981; Horne & Marsh 1986). A

comparison of the emission lines from different data sets shows that they vary not only in relative intensity but also in shape and peak-to-peak separation of the profiles. Figure 4 shows the $H\alpha$ and $H\beta$ profiles which exhibit notably different slopes of the line wings.

It is well known that the velocity-separation between peaks in the double-peaked profiles is defined by the velocity of the outer rim of the accretion disc V_{out} , which in turn depends on its radius (Smak 1981). The shape of the line wings is controlled by the surface radial emissivity profile (Smak 1981; Horne & Marsh 1986) which is commonly assumed to follow a power-law function of the form $f(r) \propto r^{-b}$, where r is the radial distance from the WD. In order to estimate accretion disc parameters, we fitted the averaged emission line profiles using a simple model of a uniform flat axisymmetric Keplerian¹ geometrically thin disc (Smak 1981; Horne & Marsh 1986). The primary free parameters of the model are

1. V_{out} , the velocity of the outer rim of the accretion disc;
2. b , the power-law index of the line emissivity profile $f(r)$;
3. r_{in}/r_{out} , the ratio of the inner to the outer radii of the disc.

Examples of the application of this technique to the real data are given in Neustroev (1998); Neustroev et al. (2002, 2014). The best-fitting model parameters for the major emission lines are listed in Table 2 and the errors were estimated with a Monte Carlo approach described in Borisov & Neustroev (1997). The model fits for the $H\alpha$ and $H\beta$ emission line profiles from the 1986, 1992 and 2005 data sets are shown in Fig. 4 by dashed lines.

Observations of CVs show that the power-law index b is usually in range of 1–2, rarely being less than 1.5 (Horne & Saar 1991). Most of our model fits also give $b \approx 1.5$ –2.0. However, the best-fitting index b for $H\alpha$ from the set-2005 is <1.0 . This suggests a flatter radial distribution of the emission-line flux from the accretion disc of HT Cas during the 2005 observations. Marsh & Horne (1990) argued that in order to explain such a behaviour, an increased role of photoionization by the soft X-rays and UV photons from the centre of the accretion disc should be taken into account. Coupled with the significantly steeper Balmer and He I decrements in the 2005 spectra, this may also suggest a lowering of gas density in an outer area of the disc producing $H\alpha$ emission.

4.4. Emission lines variations and Doppler tomography

Young et al. (1981) mentioned that the emission lines of HT Cas do not vary much in profile around the orbit (see fig. 1 in their paper). Our observations confirm this finding as well as the most mysterious property of profile variations: the blue peak of lines is stronger at phase 0.1–0.2 and the red peak is stronger near phase ~ 0.6 , that is 180° out of phase expected from the ordinary S-wave (Fig. 5). However, this is correct for the $H\alpha$ and $H\beta$ lines only, whereas the He I lines show the opposite, usual behaviour.

More details can be revealed in the trailed spectra. In top and bottom panels of Fig. 6 the most representative lines from the data sets 2005-n1 and 2005-n2 are shown. One can clearly recognize that the ordinary S-wave is certainly present in most

of the lines, yet the anomalous emission source mentioned above is strong in $H\alpha$, weaker in $H\beta$ and very weak or undetectable in He I lines. We note that even though the He II $\lambda 4686$ line is clearly seen in averaged spectra, it is still too weak and noisy to reveal any variability.

In order to provide a more convincing picture of the sources of emission in the accretion disc of HT Cas, we used Doppler tomography (Marsh & Horne 1988). For a comprehensive review of the method and many examples of its application, see Marsh (2001) and references therein. Figs. 6 and 7 show the Doppler maps computed using the code developed by Spruit (1998).

We start the discussion with the 2005 data set as these spectra have higher signal-to-noise ratio and spectral resolution and they produce maps of the best quality. The tomograms of the representative lines from this set are shown in Fig. 6, together with the corresponding reconstructed counterparts shown in the top and bottom panels, alongside with the trailed spectra. Since the gradual occultation of the emitting regions during eclipse is not taken into account, we constrained our data sets by removing eclipse spectra covering the phase ranges $\phi = 0.9$ –1.1. To help in interpreting the Doppler maps, the positions of the WD (lower cross), the center of mass of the binary (middle cross) and the Roche lobe of the secondary star (upper bubble with the cross) are marked. The predicted trajectory of the gas stream and the Keplerian velocity of the disc along the gas stream have also been shown in the form of the lower and upper curves, respectively. The Roche lobe of the secondary and the trajectories have been plotted using the system parameters, derived by Horne et al. (1991): an inclination $i=81^\circ$, mass ratio $q=0.15$ and $M_1=0.61 M_\odot$. We note that the classical two-dimensional visualization of tomograms used in Fig. 6 does not always provide adequate representation of the multi-component structure which we discuss below. We find it useful to present the Doppler map of $H\alpha$ from the set-2005-n2 also in three-dimensional (3D) form (Fig. 8).

All the Doppler maps display a ring of disc emission, which radius is different for various lines, reflecting the varied peak-to-peak velocity separation in these lines. However, the detailed appearance of the Balmer and helium tomograms is rather dissimilar. Most of the maps show a compact emission area in the fourth quadrant ($-V_x, +V_y$), which can be unequivocally identified as the hot spot located in the region of interaction between the gas stream and the outer edge of the accretion disc. This area is a dominant emission source in $H\beta$ and He I lines, but very weak in $H\alpha$. Instead, the $H\alpha$ map exhibits a bright enhanced emission region in the second quadrant ($+V_x, -V_y$) whose ambiguous nature we discuss in Section 5.3. The 3D Doppler maps of highest quality ($H\alpha$, $H\beta$, He I $\lambda 5876$) clearly show that the hot spot is located on the top of azimuthally extended emission structure of spiral shape (Fig. 8). This spiral structure in the fourth quadrant and the emission region in the second quadrant are unjoined from each other by gaps in the upper and lower-left parts of the tomograms. The Fe II $\lambda 5169$ line shows no clear evidence for neither of the three emission sources. No sign of the secondary star is seen in either tomogram.

In order to examine the stability of the emission structure of HT Cas over time, we calculated Doppler maps for the four Balmer and one He I lines from other available data sets (Fig. 7). Even though the quality of these data is notably worse than of the 2005 data set, they show the same features in Doppler maps. The main dissimilarity between observations is a different contribution of the above-mentioned components.

¹ In Section 5.1 we show that the accretion disc of HT Cas appears to have a large radius. This means that some deviations from Keplerian flow are expected at the outer disc. Steeghs & Stehle (1999) showed that the departures can reach 100 km s^{-1} . For the orbit averaged spectra, however, these deviations mostly cancel out, so the assumption of Keplerian velocities is still reliable.

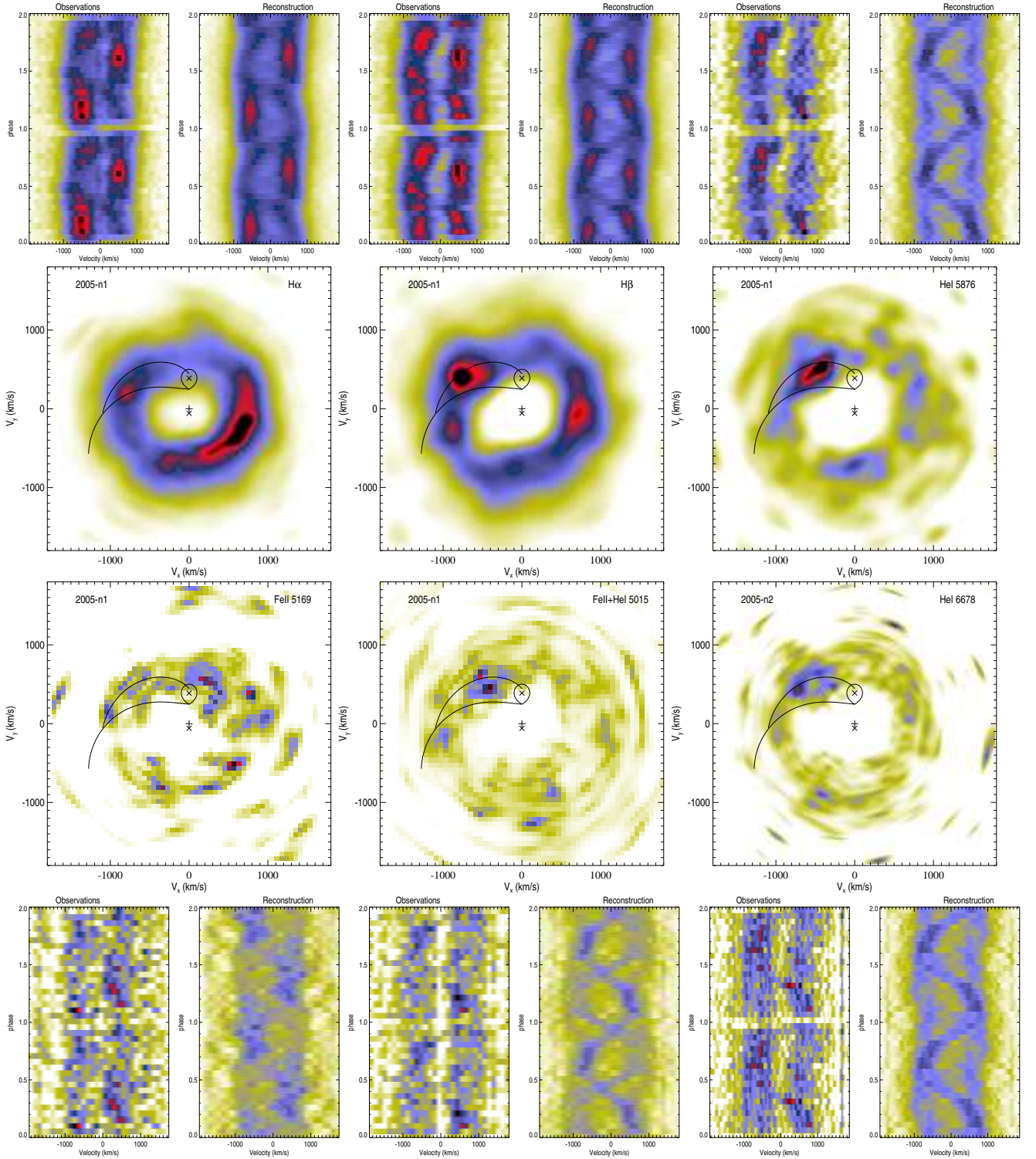


Fig. 6. Doppler tomography for the $H\alpha$, $H\beta$ and $He\text{ I } 5876$ emission lines (in the upper half of Figure), and for $Fe\text{ II } 5169$, $He\text{ I } 5015$ and $He\text{ I } 6678$ (in the bottom half of Figure) from the data sets 2005-n1 and 2005-n2. For each line the Doppler maps (two middle panels) and corresponding observed and reconstructed trailed spectra (top and bottom panels) are shown. Marked on the maps are the positions of the WD (lower cross), the center of mass of the binary (middle cross) and the Roche lobe of the secondary star (upper bubble with the cross). The predicted trajectory of the gas stream and the Keplerian velocity of the disc along the gas stream have also been shown in the form of the lower and upper curves, respectively. The Roche lobe of the secondary and the trajectories have been plotted using the system parameters, derived by Horne et al. (1991).

4.5. Radial velocity study

To the best of our knowledge, there was only one attempt to estimate the radial velocity semi-amplitude of the white dwarf in HT Cas in the past. Young et al. (1981) measured the K_1 velocity

of $115 \pm 6 \text{ km s}^{-1}$ for the emission lines, but the resulting radial velocity curve is 30° out of phase with the WD. Horne et al. (1991) showed that this result is inconsistent with most of the photometric data and predicted K_1 velocity of $58 \pm 11 \text{ km s}^{-1}$.

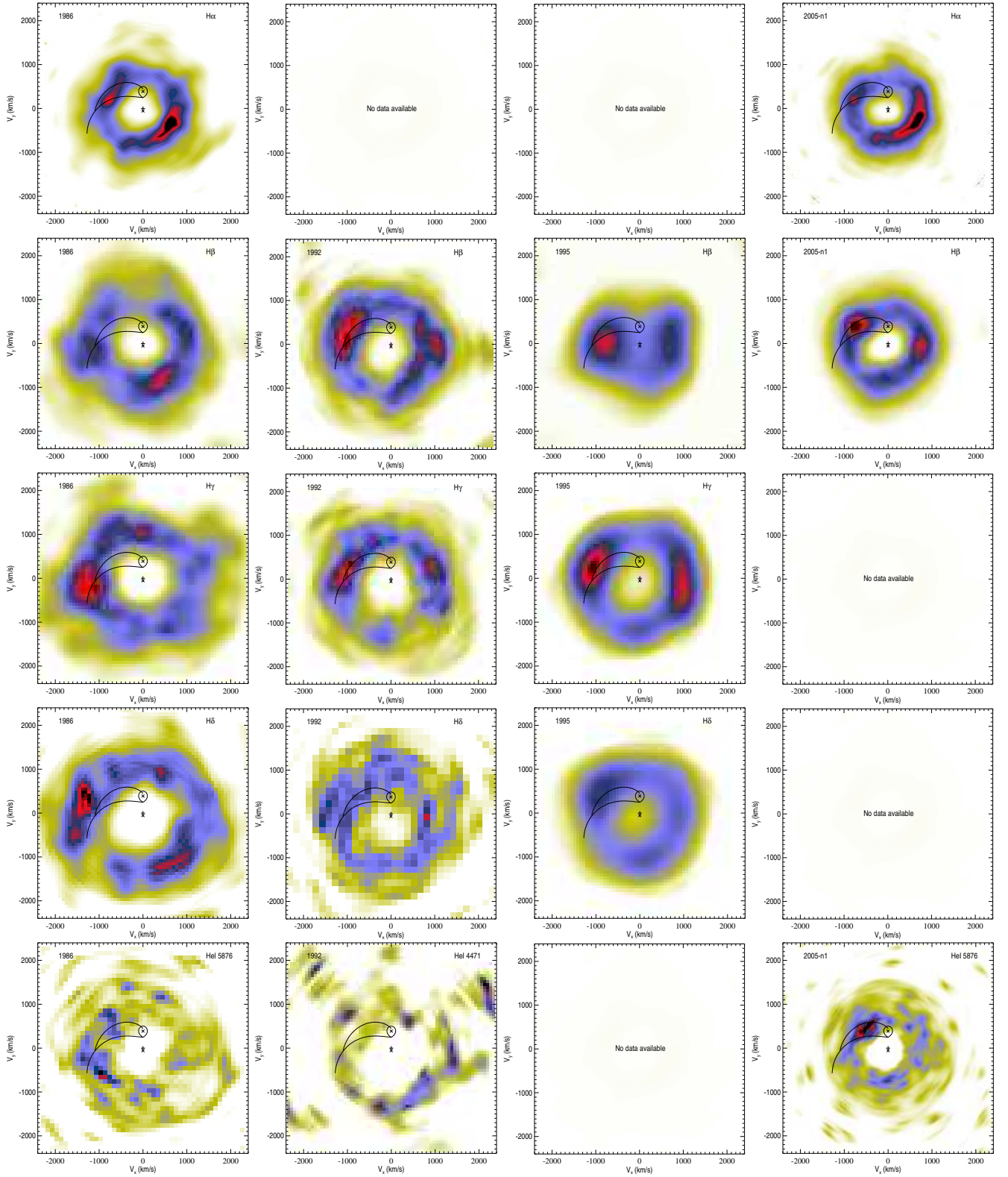


Fig. 7. Doppler tomography for the Balmer and He I emission lines. Each column shows the maps for different data sets (1986, 1992, 1995 and 2005-n1). Each row shows the maps for different lines ($H\alpha$, $H\beta$, $H\gamma$, $H\delta$ and He I).

We measured the radial velocities of the emission lines in HT Cas by applying the double-Gaussian method described by Schneider & Young (1980) and refined by Shafer (1983). This technique consists of convolving each spectrum with a pair of Gaussians of width σ whose centres have a separation of Δ . The position at which the intensities through the two Gaussians be-

come equal is a measure of the wavelength of the emission line. The measured velocities depend on the choice of Δ , and by varying its value different parts of the lines can be sampled. It is commonly believed that the most reliable parts of the emission-line profile for deriving the radial velocity curve are the extreme

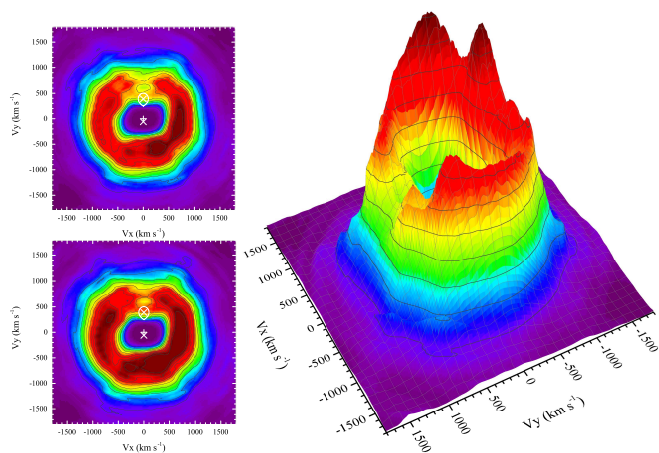


Fig. 8. Doppler map of the H α emission line from the set-2005-n2 sets in 3D (right) and 2D representations with different contrast to emphasize different components of the map (left).

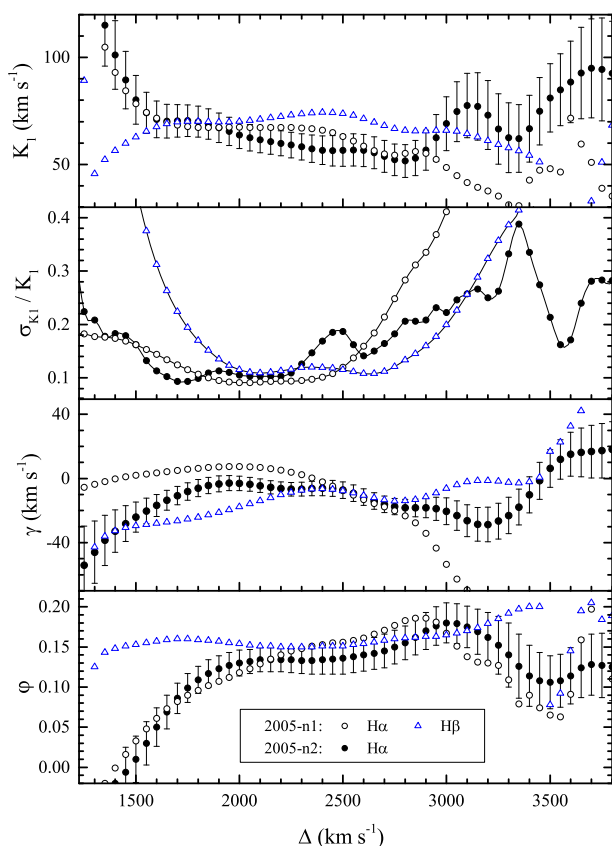


Fig. 9. The diagnostic diagram for the H α and H β emission lines from the sets 2005-n1 and 2005-n2, showing the response of the fitted orbital elements to the choice of the double-gaussian separation.

wings. Young et al. (1981) used $\Delta=3200 \text{ km s}^{-1}$ in their measurements.

In order to test for consistency in the derived velocities and the zero phase, we separately used the lines H α and H β in the set-2005-n1, and H α in the set-2005-n2. The measurements were made using the Gaussian σ of 100 and 200 km s^{-1} and different values of the Gaussian separation Δ ranging from 1200 km s^{-1} to 4000 km s^{-1} in steps of 50 km s^{-1} , following the technique of “diagnostic diagrams” (Shafter et al. 1986). For each value of Δ we made a non-linear least-squares fit of the derived velocities

to sinusoids of the form

$$V(\varphi, \Delta) = \gamma(\Delta) - K_1(\Delta) \sin [2\pi (\varphi - \varphi_0(\Delta))] , \quad (1)$$

where γ is the systemic velocity, K_1 is the semi-amplitude, φ_0 is the phase of inferior conjunction of the secondary star and φ is the phase calculated according to the ephemeris from Feline et al. (2005). During this fitting procedure we omitted spectra covering the phase ranges $\varphi = \pm 0.1$, owing to measurement uncertainties during the eclipse.

The resulting “diagnostic diagrams” are shown in Fig. 9. The diagrams show the variations of K_1 , $\sigma(K_1)/K_1$ (the fractional error in K_1), γ and φ_0 with Δ (Shafter et al. 1986). To derive the orbital elements of the line wings Shafter & Szkody (1984) suggest to take the values that correspond to the largest separation Δ_{\max} just before $\sigma(K_1)/K_1$ shows a sharp increase. We note, however, that all the parameters are consistent for different lines and are quite stable over a reasonable range of Gaussian separations around Δ_{\max} which can be set at $\sim 2500\text{--}2700 \text{ km s}^{-1}$. Using $\sigma(K_1)$, $\sigma(\gamma)$ and $\sigma(\varphi_0)$ as a weight factor, we find the following mean values of the orbital parameters: $K_1 = 61 \pm 8 \text{ km s}^{-1}$, $\gamma = -9 \pm 5 \text{ km s}^{-1}$ and $\varphi_0 = 0.15 \pm 0.02$.

The derived value of K_1 is very much consistent with the one predicted by Horne et al. (1991). However, the radial velocity curves of all the investigated emission lines are significantly shifted relative to the eclipse ($\sim 55^\circ$) and therefore these lines cannot be used to represent the motion of the WD. As seen in the diagnostic diagrams (Fig. 9), the shift is observed over the whole range of separations Δ , from emission-line profile peaks to the extreme wings where the noise begins to dominate, and its value is almost twice as large as that reported by Young et al. (1981). Though the Doppler maps of HT Cas have a very complex structure, they show no evidence for compact emission or absorption sources at the far wings of spectral lines which can be responsible for the observed phase shift in this velocity range ($>1500 \text{ km s}^{-1}$). This fact suggests that a global asymmetric configuration may exist in the inner parts of the accretion disc of HT Cas (e.g. eccentric, elliptical structure).

5. Discussion

A Doppler tomography technique applied to a large set of multi-epoch spectroscopic observations of HT Cas confirmed the guess of Young et al. (1981) about an unusual distribution of emission in this system. The tomograms show at least three areas of enhanced emission: the hot spot superposed on the spiral structure in the fourth quadrant, and the broad, extended bright region of uncertain origin in the second quadrant.

It is not possible to transform a Doppler map into a spatial map without a detailed knowledge of the velocity field. Nevertheless, for illustration purposes and to facilitate further discussion, we find it useful to show a map of the H α emission in spatial coordinates, assuming a circular Keplerian flow in the disc (Fig. 10). This assumption is not accurate in a strict sense, because some of the system components such as the gas stream do not follow a pure Keplerian rotation law. On the other hand, the assumption gives an acceptable working basis, since no significant deviation from the Keplerian rotation is expected for a thin accretion disc around the WD². This is the traditional theoretical picture of accretion discs (Shakura & Sunyaev 1973), supported

² The deviations from Keplerian flow at the outer disc (up to 100 km s^{-1}) obtained by Steeghs & Stehle (1999) are comparable with the spectral resolution of our data and the corresponding resolution of tomograms, so they cannot affect significantly the presented results.

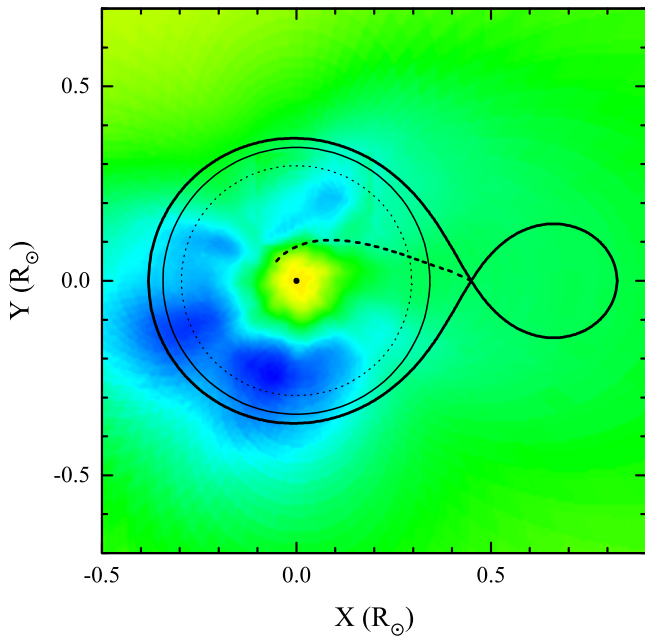


Fig. 10. The $H\alpha$ Doppler map from the 2005 observations transformed to a spatial image, assuming a circular Keplerian flow in the disc. The Roche lobes of the stars (thick solid line), the tidal truncation (thin solid line) and 3:1 resonance (thin dashed line) radii are also shown. The thick dashed line represents the gas stream from the donor star.

by observations. In the particular case of HT Cas, Young et al. (1981) presented a crude verification that the disc in this system is Keplerian over at least a factor of 4 in radius.

The accretion disc, as it appeared in Fig. 10, looks rather weird. A general impression is that the disc of HT Cas is indeed patchy, as was suggested by (Vrielmann et al. 2002). We discuss the derived structure in the following subsections.

5.1. Hot spot and the size of the accretion disc

Assuming the Keplerian velocity in the accretion disc, the measured projected outer disc velocity V_{out} can be used to determine the radius of the disc:

$$R_d = \frac{GM_1 \sin^2 i}{V_{\text{out}}^2}, \quad (2)$$

Individual spectral lines are sensitive to the local physical conditions in the disc (e.g., gas density and temperature), so different lines may lead to different apparent disc radii, reflecting the region where that particular line is excited. We measured V_{out} through the modelling of the $H\alpha$ (if it is available in the given data set) or $H\beta$ emission lines, which originate in the outermost part of the accretion disc (see Section 4.3 and Table 2). Firstly, we used the 2005 data, for which we adopted the value for V_{out} to be $575 \pm 4 \text{ km s}^{-1}$. This value is the weighted mean for the $H\alpha$ and $H\beta$ lines from the two nights, using $\sigma(V_{\text{out}})$ as a weight factor. Using the system parameters derived by Horne et al. (1991), this value gives $R_d \approx 0.52 \pm 0.01 a$.

The obtained disc radius coincides precisely with the tidal truncation radius of the accretion disc $r_{\text{max}} = 0.522a$ (for $q = 0.15$), which can be estimated using equation 2.61 from Warner 1995)

$$r_{\text{max}} = a \frac{0.6}{1 + q}, \quad (3)$$

While such a large disc is slightly tidally distorted and elongated perpendicular to the line of centres of the WD and the secondary star, the assumption of Keplerian velocities still provides a reliable estimate of the *average* disc size (see footnote 1).

A comparison of the peak-to-peak separation of emission lines from different observations including that presented by Young et al. (1981) shows that such a large disc seems to be normal for HT Cas. Most of the data (except for the 1992 observations) suggest that the accretion disc radius R_d lies within the range $0.45 - 0.52a$. This result contradicts with previous radius measurements. As we mentioned in Section 2, a typical value of R_d in quiescence was measured to be just $\approx 0.23a$. It is important to note that most of those measurements were based on the position of the hot spot (e.g., Horne et al. 1991). Our data, however, indicate that the hot spot is not located at the accretion disc edge.

Figure 11 (left-hand panel) shows a zoomed hot spot area of the map combined of all the tomograms from the 2005 observations. The position of the hot spot in all the emission lines is consistent with the trajectory of the gas stream and has a velocity close to either the expected velocity of the stream at a distance from the WD (i.e., $H\alpha$) or a Kepler velocity at the stream position ($H\beta$, He I 6678), or a mix of these velocities (He I 5876). However, the peaks of emission are located much closer to the WD ($R_{hs} \approx 0.22 - 0.30a$) than the disc edge measured from the double-peaked profiles ($R_d \approx 0.52a$). This suggests that the gas stream flows almost unaffected through the outer disc regions before it starts to be seen as a continuum and line emission source. A similar finding for the dwarf nova WZ Sge was reported by Skidmore et al. (2000) and Mason et al. (2000).

The hot spot area during the 2005 observations looks rather different in comparison to other observations. In Fig. 11 (left-hand panel) we also show the hot spot locations from the set-1986. It is interesting that the $H\alpha$ spot (marked by the red dashed line) is seen at nearly the same position as in 2005 whereas all other lines show the spot (marked by a grey oval) much further along the stream trajectory. The latter spot is also evident in Doppler maps from other data sets. This spot is still consistent with the ballistic trajectory of the gas stream, though its position is somewhat closer to the WD ($R_{hs} \approx 0.20 - 0.22a$).

During the 1992 observations the emission lines appeared notably wider in comparison with other sets of observations (see Table 2 and Fig. 4). The measured V_{out} for $H\beta$ is $742 \pm 8 \text{ km s}^{-1}$, corresponding to $R_d \approx 0.31 \pm 0.01a$. This implies that the accretion disc has significantly shrunk by about 35–40 per cent compared to other observations, even though the $H\alpha$ line is expected to be somewhat more narrow. The variability of the accretion disc radius was observed in other CVs (Warner 1995) and low-mass X-ray binaries (Neustroev et al. 2014). However, such a behaviour is usually related to outbursts in these systems, during which the disc expands dramatically and then contracts exponentially with time, whereas all the presented data of HT Cas were obtained in quiescence.

5.2. Spiral arm in the trailing side of the accretion disc

The weakness of the hot spot in the $H\alpha$ line makes it possible to trace the extended emission structure in the fourth quadrant

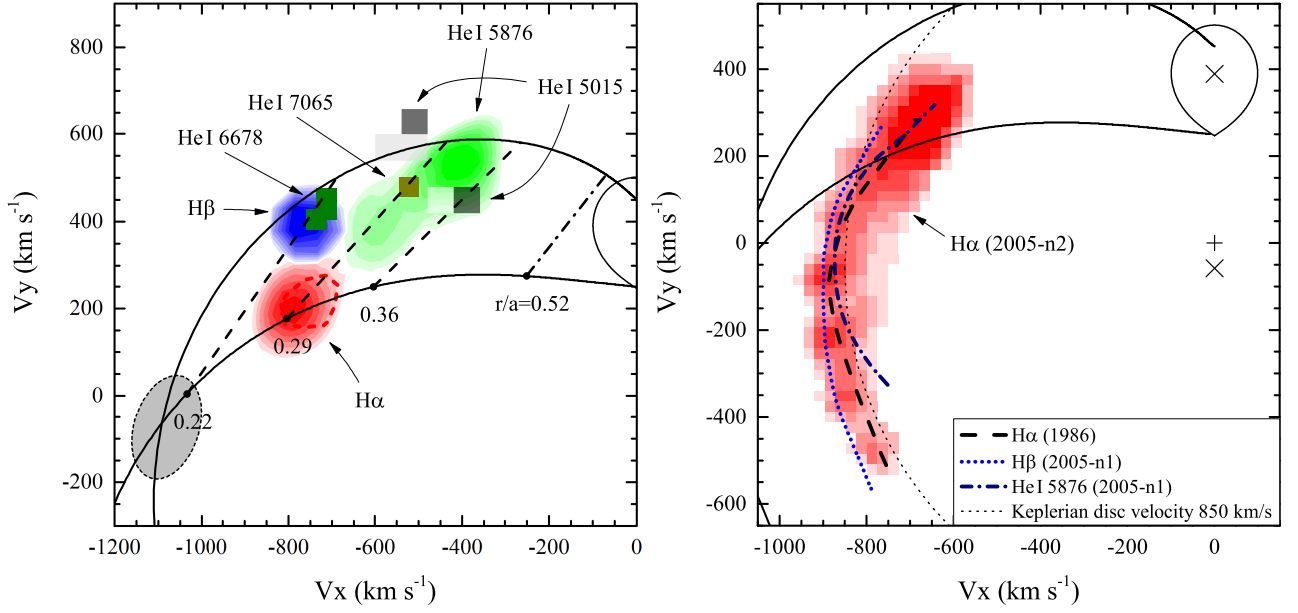


Fig. 11. Left: Zoomed hot spot area of the Doppler map combined of all the tomograms from the 2005 observations with different contrast to emphasize the hot spot location. The map also shows the spot location from the 1986 observations. The H α spot is marked by the red dashed line. A grey oval shows the other spectral lines. The dashed lines connect the velocity of the ballistic gas stream (lower curve) and the velocity on the Keplerian disc along the gas stream (upper curve) for the same points at distances labelled along the lower curve (in r/a units). The dash-dotted line corresponds to the measured radius of the accretion disc, which coincides with the tidal truncation radius $r_{\text{max}}/a=0.52$. Right: Zoomed part of the H α Doppler map from the set-2005-n2 centered around the spiral arm area. The thick lines show the trace of this area in other spectral lines and data sets. Dotted thin line shows the Keplerian disc velocity of 850 km s^{-1} .

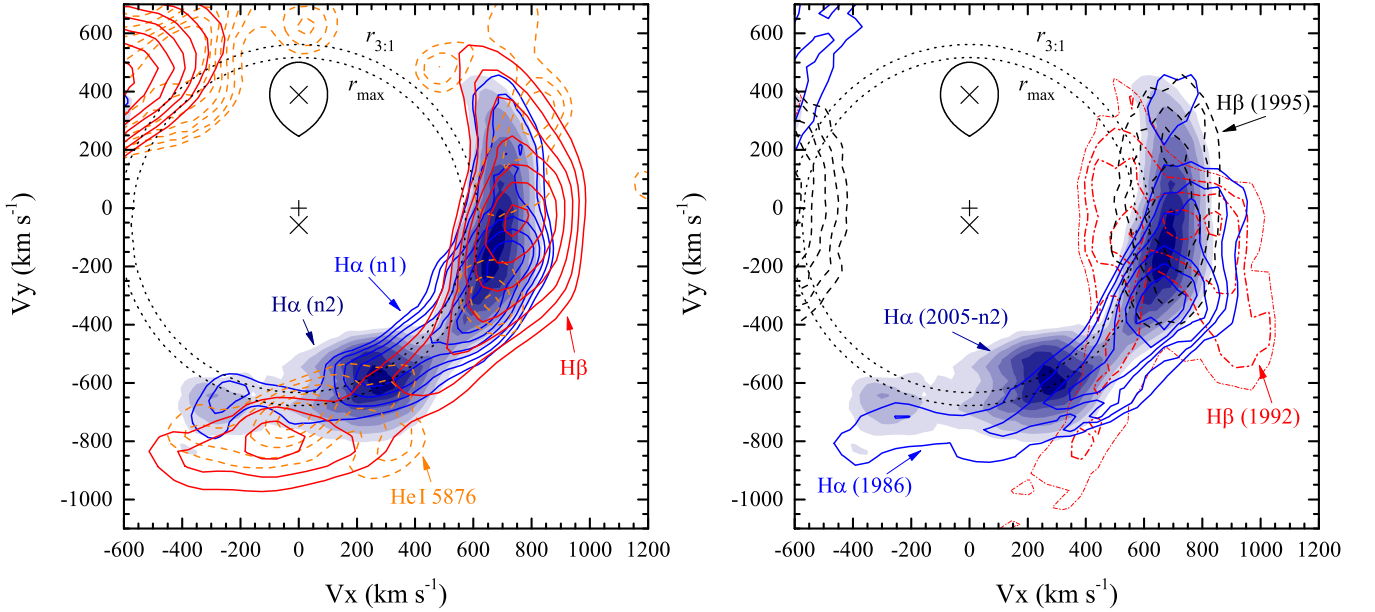


Fig. 12. Doppler maps combined of the tomograms for different lines from the 2005 observations (left) and for the strongest lines from different sets of observations (right). The maps are zoomed around the emission region in the leading side of the accretion disc. The circular dashed lines represent Keplerian velocities at the tidal truncation (r_{max}) and 3:1 resonance ($r_{3:1}$) radii.

of the tomograms in detail. Figure 11 (right-hand panel) shows a zoomed part of the H α Doppler map from the set-2005-n2 centered around this area. The latter can also be traced in other spectral lines and data sets, some of which are denoted in Figure by different lines. The location and shape of the structure is nearly the same in all the lines. It starts at the hot spot area and extends downstream in azimuth for $\sim 60^\circ$. Its width gradually decreases until this “tail” has completely disappeared.

The origin of this emission is not clear. A similar structure was observed, e.g., in WZ Sge (Spruit & Rutten 1998) and U Gem (Unda-Sanzana et al. 2006). Such a tail cannot be due to stream–disc overflow which might produce an excess of emission along the path of the stream (Kunze et al. 2001). On the other hand, a tail is to be expected as a consequence of the post-impact hydrodynamics of the gas stream and can be caused by material that has settled into Keplerian motion downstream from the hot spot (for a discussion see Spruit & Rutten 1998, and ref-

erences therein). However, despite an overall similarity of the tails in HT Cas and WZ Sge, there is a significant difference between them. The tail in WZ Sge indeed shows circular Keplerian velocities along its trail, whereas the velocity in HT Cas increases from ~ 760 to 880 km s^{-1} (Fig. 11, right-hand panel). It corresponds to the range of distances from the WD from $0.30a$ to $0.22a$ (Fig. 10). In fact, such a behaviour resembles the signature generated by spiral waves in the disc, rather than the hot spot tail in WZ Sge. However, the properties of spiral structure in the accretion discs have been particularly well studied by both numerical simulations and observations (Steehgs & Stehle 1999, and references therein), and no spiral waves or shocks are predicted in quiescent discs.

The observed spiral feature can be associated with a tidally thickened sector of the disc that is elevated due to tidal distortions and later being irradiated by the WD or inner disc (Ogilvie 2002; for a discussion see also Unda-Sanzana et al. 2006 and Section 5.3 below), though such a thickening is more expected in the outer disc than at the observed position. Another possible explanation for the spiral arm in HT Cas may come from the hydrodynamical simulations by Bisikalo et al. (1998). They showed that the gas stream may penetrate the outer disc regions, producing a so-called “hot line” (an extended shock wave) that interacts and mixes with the disc, allowing matter to be deposited at the inner disc regions.

5.3. Emission region in the leading side of the accretion disc

From Figs. 6 and 7, it may appear that the emission region in the second quadrant of tomograms is bright in the $H\alpha$ line only, and much weaker in $H\beta$ and almost undetectable in the He I lines. This impression is somewhat misleading due to the chosen contrast and colour scaling to emphasize different components of Doppler maps. We estimated the contribution of this emission source to the total flux of strongest emission lines from the set-2005 ($H\alpha$, $H\beta$ and $\text{He I } 5876$) and set-1986 ($H\alpha$ and $H\beta$) and found nearly the same value of 5–7 per cent for all of them. The region trails along the accretion disc ring for some 150° in azimuth and perhaps has a multi-component structure. The highest quality and resolution Doppler map of $H\alpha$ from the set-2005-n2 (Fig. 8) shows clearly two distinct spots of similar brightness – in the bottom and lower-right sides of the disc ring – while in some of other tomograms one of these two spots prevails over the other.

We compared the location of these structures to those found in different lines from the 2005 observations and from different sets of observations. Figure 12 shows that at least the lower-right spot is always observed in the same position (there is a weak sign of vertical shift of the bottom spot), even though the accretion disc properties differ considerably from one set of observations to another (see Section 4.1). This resembles the behaviour of another short-period CV, namely BZ UMa, in which the similar spot in the leading side of the accretion disc remained present at the same position during all stages of the outburst, from quiescence to the maximum (Neustroev et al. 2006). The velocities of the emission region suggest its origin in the outer accretion disc. The spatial map of HT Cas indicates a relatively sharp inner border of the region at $R_{b,in} \approx 0.25a$, whereas its outer parts can be traced up to the Roche lobe radius *exceeding* r_{max} (Figure 10). Though the latter property may well be an artefact of reconstruction because of the finite spectral resolution, there is no doubt that the emission comes from the outermost parts of the disc.

Neither of the bright spots, being located at the opposite side of the accretion disc, can be associated with the interaction between the gas stream and the disc. No shock waves which can produce an excess of emission in the bottom-right side of tomograms are predicted by hydrodynamical simulations, and none of the theories foresee stable shocks in the quiescent accretion disc. We propose that the leading side bright spots are caused by irradiation of relatively compact thickened sectors of the outer disc by the WD and/or hot, inner disc regions. The reason for this thickening is not clear, but can be assumed to be tidally induced. A clue to understanding the exact process can perhaps be gained from the fact that the outer parts of a large accretion disc are under the gravitational influence of the secondary star. It prevents the disc from growing above the tidal radius r_{max} , where the tidal and viscous stresses are comparable (Warner 1995). How that truncation occurs and how the disk thickness varies along the outer edge is not yet well established. To the best of our knowledge, no detailed 3D numerical simulations were devoted to these questions so far. However, Bisikalo et al. (1998) pointed out an important role of the circum-disk halo created by matter which went outside r_{max} and left the accretion disc. The accretion disc in their hydrodynamical simulations has a quasi-elliptical shape extended in a direction *opposite* to the hot spot (see also Kononov et al. 2012). Truss (2007) also reported the appearance of similarly oriented elliptical discs, though only in extreme mass ratio compact binaries ($q < 0.1$).

The asymmetry of the disc can also explain the shift of the radial velocity curve relative to inferior conjunction of the secondary star, detected in HT Cas (Section 4.5) and many other short-period CVs (Mason et al. 2000). The fact that the shift is observed in a wide range of distances from the WD suggests significantly asymmetric structures existing even in the inner parts of the disc.

5.4. Large accretion discs in cataclysmic variables

The discovery of the extended bright area in the leading side of the accretion disc of HT Cas enriches the list of objects in which such a feature was observed. Based on the large measured radius of the disc in HT Cas, we make a guess in the previous subsection that the leading side bright spot can be caused by tidally induced thickened sectors of the outer large disc. In this respect it might be worth examining if other systems showing a similar emission feature also have the large accretion disc.

We inspected several CVs with relatively well measured system parameters from the list given in Introduction and found that most of them support our idea. For example, Smith et al. (2006) reported that the disc in VW Hyi appears slightly larger than the tidal radius r_{max} . Aviles et al. (2010) and Zharikov et al. (2013) showed that the leading side spots in V406 Vir and EZ Lyn lie between the 2:1 and 3:1 resonance radii. A similar emission structure is visible in WZ Sge, for which Skidmore et al. (2000) claimed that the disc also reaches to the 3:1 resonance radius. All these systems have an orbital period shorter than the period gap for CVs. However, a few long-period CVs were also reported to show the leading side spot. One of these objects, the old nova RR Pic, displayed superhump modulations in its light curve (Schmidtobreick et al. 2008), suggesting that the disc radius is no smaller than the 3:1 resonance radius. Finally, we would like to mention famous IP Peg, which was found to display strong spiral structure in the accretion disc during outburst (Steehgs et al. 1997). It is interesting that the two bright emitting regions were occasionally observed in the Doppler maps of IP Peg also in the quiescent state. Neustroev et al. (2002) dis-

cussed them in the frame of the spiral shock model, though the location of the spots does not coincide with that observed in outburst. In fact, the tomograms of IP Peg in quiescence resemble very much the maps of HT Cas and as such IP Peg should also be included in the list of CVs with the bright spot in the leading side of the disc. Moreover, the disc radius in IP Peg, as estimated from the double-peaked emission line profiles ($\sim 570 \text{ km s}^{-1}$ – Neustroev et al. 2002), appeared to be a bit larger than the tidal truncation radius ($\approx 0.45a$ and $\approx 0.40a$, respectively).

Thus, most of the CVs with the leading side bright spot have the accretion disc, which radius is close to the tidal truncation limit. It is worth noting that at least in a few of them the radius changes little with time. For example, Mason et al. (2000) claimed that the same accretion disc radius has been observed in WZ Sge during 40 years. Our data also demonstrate that the radius of the disc in HT Cas has not changed much during all our observations, remaining persistently large. This contradicts to the modern understanding of the evolution of the accretion disc through an outburst cycle, according to which the disc expands during the outburst and then contracts with time (Warner 1995). The conclusion, that the disc radius in many short-period CVs is close or even larger than the 3:1 resonance radius, has important implications relating to the observational properties of such systems. It is expected that the accretion disc, whose radius reached the 3:1 resonance, should be tidally deformed (Osaki 1989). If it occurs during the quiescent state, then quiescent superhumps should be present in the light curve.

6. Summary

We have presented multi-epoch, time-resolved optical spectroscopic observations of the dwarf nova HT Cas, obtained during 1986, 1992, 1995 and 2005 with the aim to study the properties of emission structures in the system. Though HT Cas has always remained in quiescence, its mean brightness has changed substantially between the observations. The spectra are dominated by very strong and broad double-peaked emission lines of the Balmer series. Also numerous weaker lines of neutral helium and singly ionized iron (Fe II) are present. The high-excitation line of He II $\lambda 4686$ is clearly detected. A comparison of the averaged spectra from different data sets shows significant quantitative differences between them. There are notable variations in both emission-line strengths and their ratios for different lines, indicating a variable mix of optically thin and thick conditions. Nevertheless, these variations do not correlate with the system flux.

The emission lines are very broad with a FWZI of up to 5–6 thousand km s^{-1} and a peak-to-peak separation of $\geq 1100 \text{ km s}^{-1}$. We determined that the accretion disc radius, measured from the double-peaked profiles, is persistently large and lies within the range of $0.45\text{--}0.52a$. This is close to the tidal truncation radius $r_{\text{max}}=0.52a$ and slightly larger than the 3:1 resonance radius $r_{3:1}$ of $0.45a$. This result contradicts with previous radius measurements.

The radial velocity semi-amplitude of the WD was found to be $K_1 = 61 \pm 8 \text{ km s}^{-1}$ from the motion of the wings of the emission lines. This value is very much consistent with the one predicted by Horne et al. (1991). However, the radial velocity curves of all the investigated emission lines are significantly shifted relative to the eclipse ($\sim 55^\circ$) and therefore these lines cannot be used to represent the motion of the WD. The shift is observed from the profile peaks to the extreme wings, suggesting a global asymmetry may exist in the accretion disc of HT Cas.

An extensive set of Doppler maps has revealed a very complex emission structure of the accretion disc. Apart from a ring of disc emission, the tomograms display at least three areas of enhanced emission: the hot spot from the area of interaction between the gas stream and the accretion disc, which is superposed on the elongated spiral structure, and the extended bright region on the leading side of the disc, opposite to the location of the hot spot.

The position of the hot spot in all the emission lines is consistent with the trajectory of the gas stream. However, the peaks of emission are located in the range of distances $R_{hs} \approx 0.22\text{--}0.30a$, which are much closer to the WD than the disc edge ($0.52a$). This suggests that the outer disc regions have a very low density, allowing the gas stream to flow almost freely before it starts to be seen as an emission source. The spiral arm appears thus as a consequence of such a penetration. The stream produces an extended shock wave that interacts and mixes with the disc.

The extended emission region in the leading side of the disc has been observed in many CVs, but it had no plausible explanation until now. We have found that in all the emission lines of HT Cas this structure is always observed in the same position – at the very edge of the large disc. Observations of other CVs, which show a similar emission structure in their Doppler maps, seem to confirm this conclusion. We propose that the leading side bright region is caused by irradiation of tidally thickened sectors of the outer disc by the WD and/or hot inner disc regions.

Acknowledgements. The authors would like to thank Valery Suleimanov for the useful comments and Natalia Neustroeva for help in preparation of the manuscript. This work was supported by PAPIIT grants IN-100614 and CONACyT grants 151858 and CAR 208512 for resources provided towards this research.

References

- Aviles, A., Zharikov, S., Tovmassian, G., et al. 2010, *ApJ*, 711, 389
- Bakowska, K. & Olech, A. 2014, *Acta Astron.*, 64, 247
- Bisikalo, D. V., Boyarchuk, A. A., Chechetkin, V. M., Kuznetsov, O. A., & Molteni, D. 1998, *MNRAS*, 300, 39
- Bond, H. 1978, private communication
- Borges, B. W., Baptista, R., Papadimitriou, C., & Giannakis, O. 2008, *A&A*, 480, 481
- Borisov, N. V. & Neustroev, V. V. 1997, *Bulletin of the Special Astrophysics Observatory*, 44, 110
- Drabek, S. V., Kopylov, I. M., Somov, N. N., & Somova, T. A. 1986, *Astrofizicheskie Issledovaniia Izvestiya Spetsial'noj Astrofizicheskoi Observatorii*, 22, 64
- Feline, W. J., Dhillon, V. S., Marsh, T. R., Watson, C. A., & Littlefair, S. P. 2005, *MNRAS*, 364, 1158
- Greenstein, J. L. & Kraft, R. P. 1959, *ApJ*, 130, 99
- Heerlein, C., Horne, K., & Schwöpe, A. D. 1999, *MNRAS*, 304, 145
- Hoffmeister, C. 1943, *Astronomische Nachrichten*, 274, 36
- Honeycutt, R. K., Schlegel, E. M., & Kaitchuck, R. H. 1987, *ApJS*, 65, 451
- Horne, K. & Marsh, T. R. 1986, *MNRAS*, 218, 761
- Horne, K. & Saar, S. H. 1991, *ApJ*, 374, L55
- Horne, K., Wood, J. H., & Stiening, R. F. 1991, *ApJ*, 378, 271
- Ioannou, Z., Naylor, T., Welsh, W. F., et al. 1999, *MNRAS*, 310, 398
- Kato, T., Maehara, H., Miller, I., et al. 2012, *PASJ*, 64, 21
- Kniazev, A. Y. 1994, *SAO Report*
- Kononov, D. A., Giovannelli, F., Bruni, I., & Bisikalo, D. V. 2012, *A&A*, 538, A94
- Kraft, R. P., Mathews, J., & Greenstein, J. L. 1962, *ApJ*, 136, 312
- Kunze, S., Speith, R., & Hessman, F. V. 2001, *MNRAS*, 322, 499
- Longa-Peña, P., Steeghs, D., & Marsh, T. 2015, *MNRAS*, 447, 149
- Marsh, T. R. 1990, *ApJ*, 357, 621
- Marsh, T. R. 2001, in *Lecture Notes in Physics*, Berlin Springer Verlag, Vol. 573, *Astrotomography, Indirect Imaging Methods in Observational Astronomy*, ed. H. M. J. Boffin, D. Steeghs, & J. Cuypers, 1
- Marsh, T. R. & Horne, K. 1988, *MNRAS*, 235, 269
- Marsh, T. R. & Horne, K. 1990, *ApJ*, 349, 593
- Mason, E., Skidmore, W., Howell, S. B., et al. 2000, *MNRAS*, 318, 440
- Neustroev, V. V. 1998, *Astronomy Reports*, 42, 748

- Neustroev, V. V., Borisov, N. V., Barwig, H., et al. 2002, *A&A*, 393, 239
- Neustroev, V. V., Suleimanov, V. F., Borisov, N. V., Belyakov, K. V., & Shearer, A. 2011, *MNRAS*, 410, 963
- Neustroev, V. V., Veledina, A., Poutanen, J., et al. 2014, *MNRAS*, 445, 2424
- Neustroev, V. V., Zharikov, S., & Michel, R. 2006, *MNRAS*, 369, 369
- Ogilvie, G. I. 2002, *MNRAS*, 330, 937
- Oke, J. B. 1990, *AJ*, 99, 1621
- Osaki, Y. 1989, *PASJ*, 41, 1005
- Papadaki, C., Boffin, H. M. J., Steeghs, D., & Schmidtobreick, L. 2008, *A&A*, 487, 611
- Patterson, J. 1981, *ApJS*, 45, 517
- Rafanelli, P. 1979, *A&A*, 76, 365
- Robertson, J. W. & Honeycutt, R. K. 1996, *AJ*, 112, 2248
- Schmidtobreick, L., Papadaki, C., Tappert, C., & Ederoclite, A. 2008, *MNRAS*, 389, 1345
- Schmidtobreick, L., Tappert, C., & Saviane, I. 2003, *MNRAS*, 342, 145
- Schneider, D. P. & Young, P. 1980, *ApJ*, 238, 946
- Shafter, A. W. 1983, *ApJ*, 267, 222
- Shafter, A. W. & Szkody, P. 1984, *ApJ*, 276, 305
- Shafter, A. W., Szkody, P., & Thorstensen, J. R. 1986, *ApJ*, 308, 765
- Shakura, N. I. & Sunyaev, R. A. 1973, *A&A*, 24, 337
- Skidmore, W., Mason, E., Howell, S. B., et al. 2000, *MNRAS*, 318, 429
- Smak, J. 1969, *Acta Astron.*, 19, 155
- Smak, J. 1970, *Acta Astron.*, 20, 311
- Smak, J. 1981, *Acta Astron.*, 31, 395
- Smith, A. J., Haswell, C. A., & Hynes, R. I. 2006, *MNRAS*, 369, 1537
- Spruit, H. C. 1998, *ArXiv Astrophysics e-prints* [astro-ph/9806141]
- Spruit, H. C. & Rutten, R. G. M. 1998, *MNRAS*, 299, 768
- Steeghs, D., Harlaftis, E. T., & Horne, K. 1997, *MNRAS*, 290, L28
- Steeghs, D. & Stehle, R. 1999, *MNRAS*, 307, 99
- Tappert, C. & Hanuschik, R. 2001, in *Lecture Notes in Physics*, Berlin Springer Verlag, Vol. 573, *Astrotomography, Indirect Imaging Methods in Observational Astronomy*, ed. H. M. J. Boffin, D. Steeghs, & J. Cuypers, 119
- Tappert, C., Mennickent, R. E., Arenas, J., Matsumoto, K., & Hanuschik, R. W. 2003, *A&A*, 408, 651
- Truss, M. R. 2007, *MNRAS*, 376, 89
- Unda-Sanzana, E., Marsh, T. R., & Morales-Rueda, L. 2006, *MNRAS*, 369, 805
- Verbunt, F. & Rappaport, S. 1988, *ApJ*, 332, 193
- Vrielmann, S., Hessman, F. V., & Horne, K. 2002, *MNRAS*, 332, 176
- Warner, B. 1995, *Cambridge Astrophysics Series*, 28
- Wenzel, W. 1987, *Astronomische Nachrichten*, 308, 75
- Williams, G. 1983, *ApJS*, 53, 523
- Wood, J. H., Horne, K., & Vennes, S. 1992, *ApJ*, 385, 294
- Wood, J. H., Naylor, T., Hassall, B. J. M., & Ramseyer, T. F. 1995, *MNRAS*, 273, 772
- Yakin, D. G., Suleimanov, V. F., Borisov, N. V., Shimanskii, V. V., & Bikmaev, I. F. 2011, *Astronomy Letters*, 37, 845
- Young, P., Schneider, D. P., & Sackett, S. A. 1981, *ApJ*, 245, 1035
- Zhang, E.-H., Robinson, E. L., & Nather, R. E. 1986, *ApJ*, 305, 740
- Zharikov, S., Tovmassian, G., Aviles, A., et al. 2013, *A&A*, 549, A77